Performance analysis of a scalable solar-assisted pilot scale adsorption desalination and cooling system

Energy Conversion and Management 343 (2025) 120190

Contents lists available at ScienceDirect

Energy Conversion and Management

journal homepage: www.elsevier.com/locate/enconman

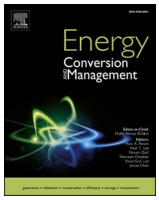

Research Paper

Performance analysis of a scalable solar-assisted pilot scale adsorption desalination and cooling system

Ali Naeimi Tabasian [a,b], Alberto Saija [c], Matteo Morciano [b,c], Matteo Fasano [b,c,*], Alberto Tiraferri [a,b], Eliodoro Chiavazzo [b,c]

[a] Department of Environment, Land and Infrastructure Engineering (DIATI), Politecnico di Torino, Corso Duca degli Abruzzi 24, 10129 Torino, Italy
[b] Clean Water Center, Politecnico di Torino, Corso Duca degli Abruzzi 24, 10129 Torino, Italy
[c] Department of Energy "Galileo Ferraris" (DENERG), Politecnico di Torino, Corso Duca degli Abruzzi 24, 10129 Torino, Italy

ARTICLE INFO

Keywords:
Adsorption desalination
Solar energy
Cooling production
Pilot plant
Silica gel

ABSTRACT

Adsorption desalination has emerged as a promising alternative to conventional methods due to its compatibility with low-grade heat sources. This study evaluates the performance of a solar-assisted, 2-bed mode pilot-scale adsorption desalination system utilizing silica gel as adsorbent material. This system adopts a new droplet-based mechanism of feed and distillate water distribution between the tanks and the adsorption beds to ease the water vapor transfer as a possible solution to prevent a reduction of specific productivity as the system scale increases. The evaluated key performance metrics include specific daily water production, specific cooling production, coefficient of performance, and overall conversion ratio. The adsorbent material was characterized, and an appropriate isotherm model suggested to predict water adsorption. System performance was assessed under varying desorption temperatures provided by a solar water heater and different cycle durations. At a desorption temperature of 70 °C and a cycle duration of 30 min, the system achieved a water production capacity of approximately 3.8 $m^3 \cdot ton^{-1} \cdot day^{-1}$ and a cooling capacity of 100 $W \cdot kg^{-1}$. Increasing the cycle duration led to improved performance metrics, although the rate of improvement decreased progressively. Additionally, the conversion ratio was maximized at desorption temperatures above 68 °C and cycle durations longer than 46 min, indicating thermodynamic efficiency. Overall, the system demonstrated promising performance as a scalable and sustainable solution for solar-assisted adsorption desalination.

1. Introduction

The global demand for freshwater is growing, fueled by population growth and economic expansion, creating an urgent challenge for sustainable water management. Despite water covering 70 % of Earth's surface, 97 % of it is seawater, unsuitable for direct use in agriculture, industry, or households due to its high salinity (35,000 TDS). Freshwater constitutes a mere 3 %, with much of it locked in glaciers or underground. Climate change intensifies this crisis, particularly in semi-arid regions, underscoring the critical need for efficient desalination technologies [1,2].

Over the years, a range of desalination methods have been developed to address this challenge. Conventional techniques include thermal processes, such as multi-stage flash (MSF), multi-effect distillation (MED), and mechanical vapor compression (MVC), as well as non-thermal methods like reverse osmosis (RO), which dominates 63 % of global desalination capacity [3,4]. However, these methods face important limitations, including unsustainable energy source, namely, electricity or high-temperature streams, as well as fouling, scaling, and constraints on feed salinity and recovery rates [5]. Emerging technologies, like freezing desalination, solvent extraction and hybrid membrane-based systems, aim to overcome these challenges [6–9]. Among these, adsorption desalination (AD) is gaining momentum as a low-maintenance solution that can effectively utilize waste heat or renewable energy [10]. Patented in 2005, AD uses hydrophilic adsorbents to adsorb water vapor from a low-pressure environment, thus providing the driving force for evaporation, offering high recovery rates and integrated cooling capabilities, the latter expanding its range of applications beyond freshwater production [10,11]. Research has explored various adsorbent materials, such as silica gel, zeolites, and metal–organic frameworks, and system configurations to enhance performance. These include optimizing the number of beds, process timing, stages, and heat recovery schemes [12]. A comparison of key

* Corresponding author at: Clean Water Center, Politecnico di Torino, Corso Duca degli Abruzzi 24, 10129 Torino, Italy.
E-mail address: matteo.fasano@polito.it (M. Fasano).

https://doi.org/10.1016/j.enconman.2025.120190
Received 12 February 2025; Received in revised form 3 July 2025; Accepted 7 July 2025
Available online 11 July 2025

Nomenclature

C	Equilibrium water uptake, $[kg \cdot kg^{-1}]$
C_0	Pre-exponential factor, $[kg \cdot kg^{-1}]$
C_p	Specific heat capacity, $[J \cdot kg^{-1} \cdot K^{-1}]$
COP	Coefficient of performance, [−]
E	Characteristic energy of adsorbent, $[J \cdot mol^{-1}]$
h_{fg}	Latent heat of evaporation, $[J \cdot kg^{-1}]$
M	Mass, [kg]
$\dot{m}$	Mass flowrate, $[kg \cdot s^{-1}]$
n	Surface heterogeneity factor, [−]
OCR	Overall conversion ratio, [−]
P	Pressure, [Pa]
P_0	Saturation pressure, [Pa]
Q	Power, [W]
ρ	Density, $[kg \cdot m^{-3}]$
R	Universal gas constant, $[J \cdot mol^{-1} \cdot K^{-1}]$
SCP	Specific cooling power, $[W \cdot kg^{-1}]$
$SDWP$	Specific daily water production, $[m^3 \cdot ton^{-1} \cdot day^{-1}]$
t	time, [s]
T	Temperature, [K]
V	Volume, $[m^3]$

Subscripts

ads	Adsorbent/Adsorption
cond	Condenser/Condensation
cycle	Adsorption cycle (Adsorption + Desorption)
des	Desorption
evap	Evaporator/Evaporation
hw	Hot water
w	Water

Superscripts

in	Inlet
out	Outlet

desalination technologies in terms of energy consumption and production costs is shown in Table 1. When comparing the adsorption desalination system to conventional technologies, it is important to note that the performance metrics reported for adsorption desalination in the literature often assume that the low-grade thermal energy required for desorption is freely available, typically from solar or waste heat sources [13,14]. Therefore, the energy consumption includes only the electrical energy reported to be about 1.38 $kWh \cdot m^{-3}$ and leading to a production cost of 0.3 $\$ m^{-3}$ [2].

Extensive studies have demonstrated AD's potential to optimize water production and energy efficiency. For example, Wang and Ng [10] investigated a 4-bed system, achieving an optimal water production of 4.7 kg per kilogram of adsorbent with a cycle time of 180 s, and highlighted the negative effects of higher bed and evaporator temperatures on performance. Thu et al. [16] introduced a novel heat recovery configuration that recycled condenser heat for water evaporation, eliminating cooling production but substantially increasing daily water production to 9.24 m^3 per ton of adsorbent at 70 °C. Ng et al. [17] proposed a "master and slave" 4-bed configuration, which alternated primary and secondary adsorption phases, achieving a specific daily water production (SDWP) of 8 m^3. Similarly, Youssef et al. [18] found that maintaining low condenser temperatures (10 °C) alongside higher evaporator temperatures (30 °C) maximized SDWP at 10 m^3. Studies by Wu et al. [11,19] confirmed the importance of temperature gradients, showing that evaporator temperatures below the cooling bed temperature enhanced water production.

Mitra et al. [20] identified an optimum cycle duration for single-stage adsorption desalination to maximize water production. Thu et al. [21] demonstrated that internal heat recovery could triple production compared to conventional systems, achieving 8.1 m^3 SDWP at 50 °C without cooling, and later [22] proposed a 3-bed, dual-pressure configuration that increased water uptake and provided two cooling grades. Youssef et al. [23] found that AQSOA-02 outperformed silica gel in water and cooling production below 20 °C, with silica gel being superior above this threshold; they further [18] demonstrated AQSOA-02's flexibility in dual-cycle systems for varying desalination and cooling demands. Ali et al. [24] proposed a 4-bed, 2-evaporator system with optimized timing, increasing production by 45 %. Naeimi et al. [25] combined heat recovery with dual integrated 4-bed cycles, achieving 9.6 m^3 production while partially maintaining cooling. Amirfakhraei et al. [26] showed that cold water temperatures had twice the effect of hot water on the coefficient of performance (COP) in a recovery scheme. Ma et al. [27] found heat recovery between adsorption and desorption beds improved energy efficiency without increasing water production, maintaining 4.69 m^3 SDWP but boosting the performance ratio. Lastly, Bai et al. [28] highlighted the negative impact of higher feed water salinity on both desalination and cooling performance.

Innovative approaches to AD have also explored solar energy integration and hybrid configurations to improve sustainability. Du et al. [29] optimized solar panel area for such systems, demonstrating that using an optimized collector area could reduce the unit cost of freshwater production by 20 % when auxiliary energy is expensive. They calculated the overall cost of solar heating for adsorption desalination to be between 0.03 and 0.04 CNY MJ^{-1}, lower than other energy sources. Ali et al. [30] investigated the performance of a solar-driven hybrid adsorption desalination system in Egypt, showing that increased daily solar radiation enhanced production capacities and confirming the region's suitability for solar-powered desalination. Similarly, Alsaman et al. [31] designed and tested a solar adsorption desalination and cooling system in the Egyptian climate, achieving 112 $W \cdot kg^{-1}$ of cooling power and an average daily water production of 4 m^3.

Building on these foundations, this study evaluates the feasibility of a solar-powered, pilot-scale AD system that integrates both adsorption desalination and cooling—exploiting the synergy between the two processes. Using silica gel as the adsorbent, it examines performance under varying operational conditions, focusing on hot water temperature and cycle duration. To enhance water vapor transfer and improve overall efficiency, we introduce a novel droplet-based feed and distillate water circulation mechanism between the tanks and the side sections of the adsorption beds, which potentially ease future scalability. By

Table 1
Comparison of conventional desalination technologies in terms of energy consumption and unit production cost [15].

Desalination method	Energy consumption (kWh m^{-3})	Unit production cost[a] ($ m^{-3})
Reverse osmosis (RO)	2–6	0.85
Multi stage flash (MSF)	12.5–24	1.6
Multi effect distillation (MED)	7.7–21	1.25
Electrodialysis (ED)	7–15	0.97

[a] Note that the production cost depends strongly on the location due to, e.g., differences in wide differences in energy, labor, materials costs, and other factors.

facilitating evaporation and condensation within these side sections, the system reduces in a substantial way the water vapor transfer resistance compared to systems discussed in the literature. Through an in-depth evaluation of water production, cooling output, and thermodynamic efficiency, this research furthers the development of sustainable, cost-effective technologies that can scale to meet water and cooling needs in arid regions.

2. Materials and methods

2.1. Adsorbent material

The adsorbent material utilized in the system was a highly-porous and amorphous form of silica gel ($SiO_2{\cdot}nH_2O$) known commercially as "Siogel", manufactured for dehumidification applications by Oker-Chemie GmbH (Goslar, Germany). The material has an internal surface area as high as 800 $m^2{\cdot}g^{-1}$, enabling excellent capacity for water adsorption. This low-cost and widely available material can be regenerated at a relatively lower temperature, compared to other materials typically used as water adsorbents, such as zeolites and activated alumina [32]. A qualitative comparison between silica gel, zeolite, and MOFs is presented in the Table S.1 of the Supplementary Information (SI) [12]. The key properties of the material utilized in this work are summarized in Table 2.

The adsorbent particles were characterized with a vapor sorption analyzer (SPSx-1μ from ProUmid GmbH & Co. KG, Ulm, Germany; see photographs and the example of a sample report in Figs. S.1 and S.2 of the SI). The adsorption capacity was measured at several temperatures and relative humidity levels. The sorption behavior was analyzed two times, the first by increasing the relative humidity of the environment from 0 % to 100 %, and then by reversing the path to determine both the adsorption and desorption behavior of the material and measure the hysteresis. The resulting data were then fitted to an isotherm model. According to the literature [31], the Dubinin-Astakhov (D-A) isotherm is an accurate predictor for the water sorption behavior of silica gel and it was thus selected in this study. The D-A isotherm equation is as follows [33,34],

$$C = C_0 \exp\left(-\left(\frac{RT}{E}\ln\left(\frac{P_0}{P}\right)\right)^n\right). \left[kg{\cdot}kg^{-1}\right] \quad (1)$$

Here, C is the equilibrium water uptake, C_0 the pre-exponential factor, R the universal gas constant, T the temperature, E the characteristic energy of adsorbent, P_0 the saturation pressure, P the pressure, and n the surface heterogeneity factor.

2.2. Adsorption desalination system, testing protocol, and performance evaluation

The pilot adsorption desalination plant utilized in this work (manufactured by Sorption Technologies GmbH), presented in Figs. 1 and 2, is divided into two main sections. The first section (Fig. 2a) is located indoor and consists of two equivalent adsorption units, each packed with 15 kg of Siogel beads, along with one feed tank and one distillate tank, each equipped with internal coils, and two circulation pumps. The second section (Fig. 2b and c) is partly located outdoor and serves as energy supply/sink units, including a vacuum tubes solar panel, a heat storage tank, a dry cooler, and a water/glycol heat exchanger.

Table 2
Characteristics of the porous adsorbent silica manufactured by Oker-Chemie GmbH.

Name	Siogel
Formula	$SiO_2{\cdot}nH_2O$
Grain size	0.5–1.5 mm
Internal surface area	800 $m^2{\cdot}g^{-1}$

Each adsorption unit includes an adsorption bed – which hosts Siogel beads – and two droplet-based evaporation/condensation systems. Each droplet-based evaporation/condensation system is made of a perforated liquid distributor, polymeric Pall rings, and a separation polymeric mesh, which enhances heat and mass transfer while preventing liquid intrusion into the adsorption bed. The adsorption unit operates with two alternating droplet systems: one for evaporation, where feedwater drips downward, fragments through Pall rings, and evaporates under low pressure, leaving concentrated feedwater (see Fig. 2d); and one for condensation, where the inlet distillate follows a similar process to condense water vapor (see Fig. 2e). This cyclic mechanism enables continuous desalination with high efficiency. Unlike conventional systems for adsorption desalination, this system physically separates evaporation and condensation from the adsorption bed, ensuring greater stability and precise phase control. In principle, its modular design allows scalability without compromising performance, while the adopted polymeric materials enhance durability, corrosion resistance, adaptability to harsh feedwaters, and lower thermal inertia thus fast response to thermal inputs, making it ideal for renewable heat sources (as detailed in the US patent n. US20220390154A1).

After a preparation stage, the system performs water desalination in cycles, during which each of the two adsorption units goes under different steps of precooling, adsorption, preheating, and desorption. This configuration ensures that while one unit is in the adsorption phase, the other one is in the desorption phase, with the goal of providing a continuous water output. Two circulation pumps controlled by pneumatic valves connect the feed and distillate tanks to the adsorption units. The heating and cooling circuits of the units are connected to the outdoor section of the system via the heat storage tank and water/glycol heat exchangers. The heat storage tank is heated up through an internal circuit connected with the solar panel, supplemented by an electric resistance to compensate for any additional energy needs. Another water/glycol circuit keeps the cooling water of the system at low temperatures, using a heat exchanger and a dry cooler unit. The plant is equipped with multiple sensors for monitoring and control. Temperature sensors/transmitters are installed at the inlet and outlet points of the heating and cooling circuits to the adsorption units, the heat storage tank, and the feed and distillate tanks. A pressure sensor/transmitter measures the bed pressure continuously. Moreover, the feed and distillate tank level meters measure the level of water in the tanks. Finally, an electrical conductivity meter was installed on the distillate tank to monitor the product water quality. All measurement data were monitored via a unified computer interface. Heating and cooling temperature, as well as cycle duration, are free operational parameters and were controlled at the desired value. The system specification, geometry, and conditions are summarized in Table 3.

The system operates in a semi-continuous mode, comprising two main stages, (i) system preparation and (ii) the main cyclic desalination process. In the preparation stage, the feed water (in this work, tap water) is charged fully into the feed tank, while the distillate tank is filled with a specific amount of distilled water for circulation and temperature control. All the pneumatic valves connecting the adsorption units to the feed and distillate tanks are opened, and a pump creates vacuum in the system. After reaching the desired vacuum level, the valves are closed, and the system is ready for the desalination stage. This stage begins upon setting the operating conditions, such as cycle duration, temperature setpoints, and pump speed. During the desalination stage, each adsorption bed goes through the following steps in a cyclic manner:

2.2.1. Precooling phase

As the bed is isolated from both the feed tank and the distillate tank, the cooling water runs through the bed's internal circuit to lower its temperature. The target is to cool down the adsorption bed along an isosteric path and prepare it for the subsequent adsorption phase.

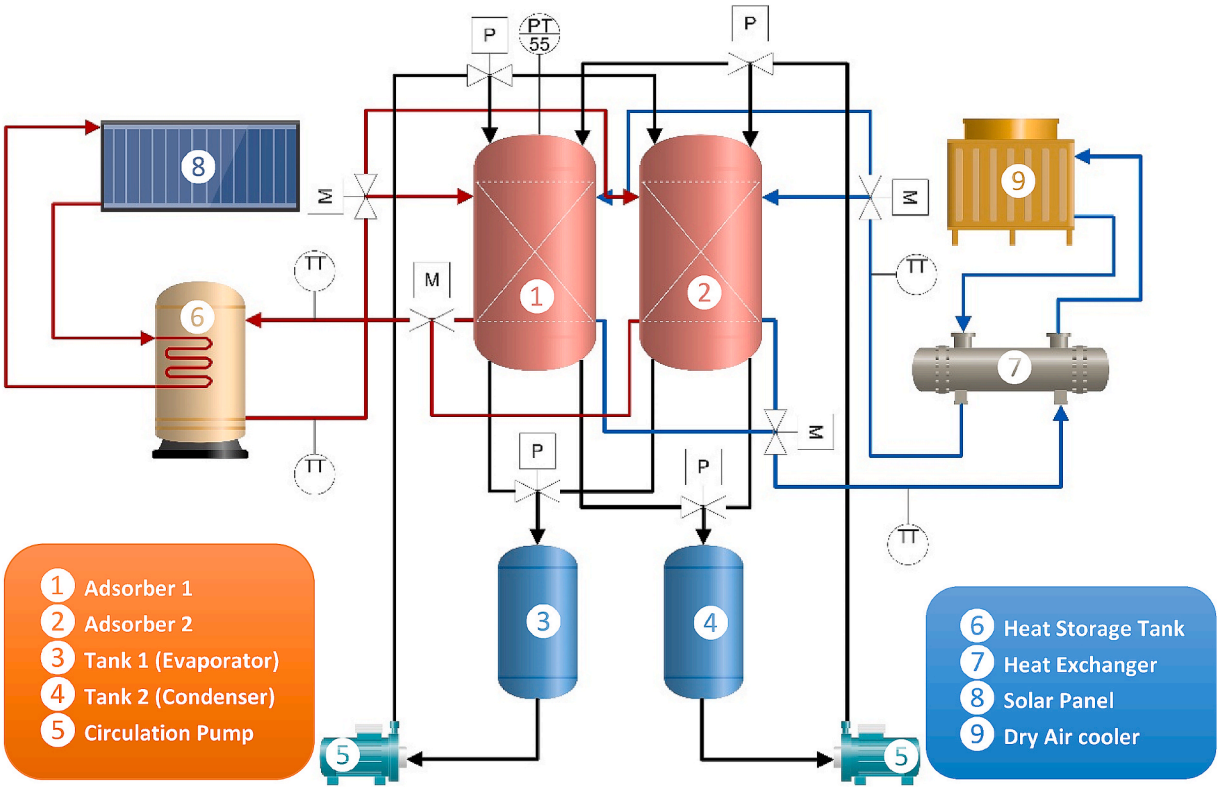

Fig. 1. Schematic of the pilot adsorption desalination system consisting of a main adsorption cycle equipment, heat supply/sink components, and circulation units.

2.2.2. Adsorption phase

While the cooling water is still running through the bed circuit, the connection between the adsorption unit and the feed tank opens, and a circulation pump starts to run the feed water through the evaporation side of the unit (see Fig. 2d). This creates droplets falling from the top to the bottom side of the unit throughout the Pall rings. During this step, as water evaporates from the droplets, the vapor is adsorbed by the sorbent material while the generated heat is removed by the cooling circuit. The evaporation also cools down the droplets returning to the feed tank. Therefore, to control the tank temperature, a portion of the hot water circulates automatically inside an internal coil within the feed tank, whenever required. The phase continues for a preset duration, selected based on the adsorption kinetics of the material.

2.2.3. Preheating phase

The adsorption unit is isolated once again, and the cooling water is replaced with heating water from the heat storage tank to increase the bed's temperature and prepare it for the subsequent desorption phase. Analogous to the precooling step, but in the opposite way, this phase aims to transition the bed along an isosteric path.

2.2.4. Desorption phase

Finally, the connection between the adsorption unit and the distillate tank opens, and the other circulation pump runs the distilled water. The high-temperature water in the bed internal circuit provides the energy for water vapor to desorb from the adsorbent material. The desorbed vapor condenses on the liquid droplets in the distillate side (see Fig. 2e) and is collected as freshwater in the distillate tank. The condensation increases the temperature of the circulating distillate water and, in turn, that of the distillate water tank. In a similar way to the feed tank, to control the distillate water tank temperature and maintaining the condensation rate constant, the cooling water from the dry air cooler circulates inside an internal coil within the distillate tank (after passing through the other bed, which is working in the adsorption phase). This phase continues for a preset duration and the cycle repeats.

The timetable of the desalination stage for both beds is presented in Fig. 3. At every instant, one bed is in the desorption step, thus achieving continuous water production. The process continues until a point when the level of seawater in the feed tank is lower than the threshold level needed to be in contact with the internal coil for tank temperature control. Therefore, the feed and product waters are discharged, and the process can be repeated starting from the preparation stage.

To evaluate the performance of the adsorption desalination system, four AD conventional indicators were taken from literature [18] and calculated for the current system, namely, the specific daily water production (SDWP) to determine the desalination capacity, the specific cooling power (SCP) and the coefficient of performance (COP) for evaluating the cooling capacity, and finally the overall conversion ratio (OCR) to analyze the thermodynamic efficiency of the system (the ratio of combined desalination and cooling powers produced by the system to the required power input of the system for desorption), defined as follows,

$$SDWP = \frac{\Delta V_{cond}}{M_{ads}\Delta t}\left[\mathrm{m^3{\cdot}ton^{-1}{\cdot}day^{-1}}\right] \tag{2}$$

$$SCP = \frac{Q_{evap}}{M_{ads}}\left[\mathrm{W{\cdot}kg^{-1}}\right] \tag{3}$$

$$COP = \frac{Q_{evap}}{Q_{des}}[-] \tag{4}$$

$$OCR = \frac{Q_{evap} + Q_{cond}}{Q_{des}}[-] \tag{5}$$

where ΔV_{cond} is the volume of desalinated water, Δt the duration of the process, M_{ads} the mass of adsorbent, Q_{evap} the heat power of evaporation, Q_{des} the heat power of desorption, and Q_{cond} the heat power of condensation. The heat powers of evaporation, desorption, and condensation can be calculated as follows:

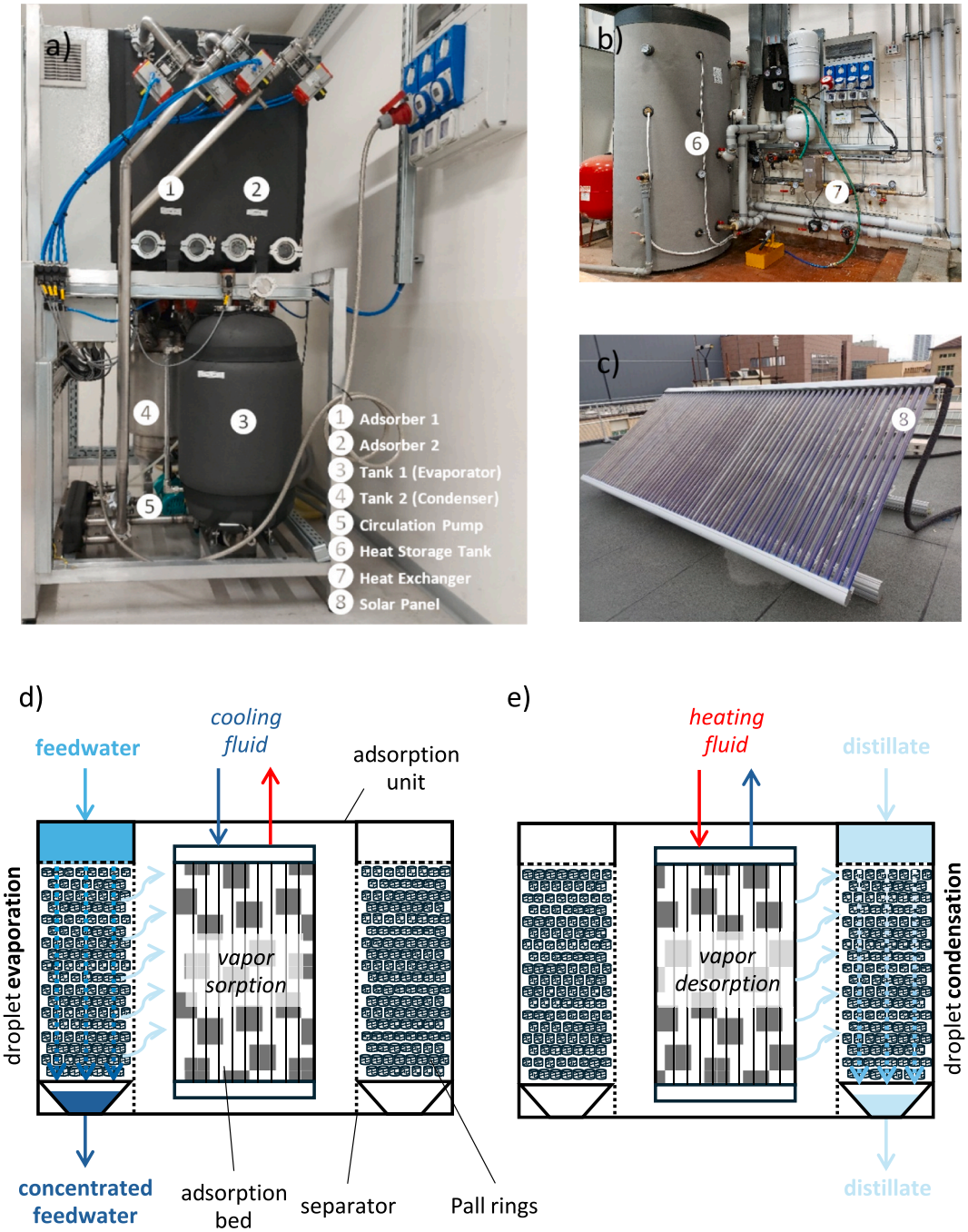

Fig. 2. Picture of the pilot plant setup for adsorption desalination including: a) the main indoor desalination components; b) the indoor heat storage tank and heat exchanger; c) outdoor solar panel. Detailed schematic of each adsorption units during the d) adsorption or e) desorption phase.

Table 3
The adsorption desalination system specification, geometry and test operating conditions.

Adsorbent mass (each bed)	15 kg
Feed water tank volume	50 L
Feed water salinity (electrical conductivity)	554 $\mu S \cdot cm^{-1}$
Hot water temperature	60 °C
Cold water temperature	25 °C
Hot water flowrate	18.3 $L \cdot min^{-1}$
Cold water flowrate	26.7 $L \cdot min^{-1}$
Cycle duration	50 min
Heat storage tank volume	856 L

$$Q_{evap} = \frac{\Delta V_{evap} \rho_w h_{fg}}{\Delta t} \text{[W]} \quad (6)$$

$$Q_{des} = \frac{1}{t_{cycle}} \int_0^{t_{cycle}} \dot{m} C_p \left(T_{hw}^{in} - T_{hw}^{out}\right) dt \text{ [W]} \quad (7)$$

$$Q_{cond} = \frac{\Delta V_{cond} \rho_w h_{fg}}{\Delta t}. \text{ [W]} \quad (8)$$

Here, ΔV_{evap} is the volume of evaporated water from the feed tank, ρ_w the water density, h_{fg} the latent heat of evaporation, t_{cycle} the cycle duration, $\dot{m}$ the mass flowrate of hot water circulation in the adsorption bed, C_p the specific heat capacity of water, T_{hw}^{in} the hot water bed inlet

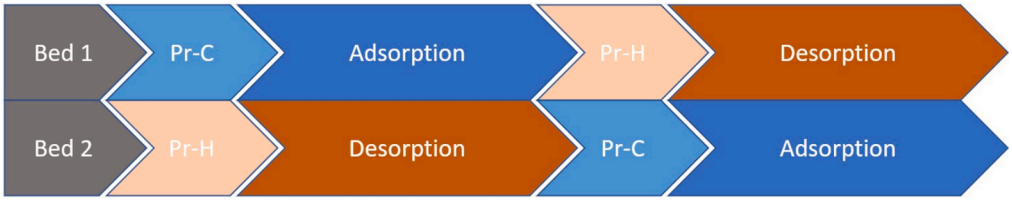

Fig. 3. Timetable of the adsorption desalination process for each adsorption bed. "Pr-C" and "Pr-H" abbreviations stand for precooling and preheating, respectively.

temperature, T_{hw}^{out} the hot water bed outlet temperature, and ΔV_{cond} the volume of condensed (product) water in the distillate tank.

3. Results and discussion

3.1. Adsorbent material behavior

The results of the adsorbent characterization and isotherm modeling are presented in Fig. 4. The data for water uptake on the adsorbent material are plotted as a function of adsorption potential, highlighting the predictable reduction in adsorption capacity with increasing temperature. The D-A isotherm was then utilized to fit the data, which resulted in regression parameters reported in Table 4. The D-A isotherm adequately describes the water adsorption behavior of the Siogel material.

3.2. Performance of desalination

The experimental results of a representative test of the adsorption desalination process, conducted at a desorption temperature of 60 °C and cycle duration of 50 min, are presented in Fig. 5. Fig. 5a displays the temperature transients of the adsorption beds, the feed tank (evaporator), and the distillate tank (condenser), while Fig. 5b illustrates the corresponding pressure.

Focusing on adsorption bed #1 (dashed orange line in Fig. 5a), a rapid decrease in its temperature can be observed at the start of the process (dimensionless time = 0). This marks the precooling phase, during which the bed was isolated, and cooling water circulated through its internal circuit, lowering its temperature. As the adsorption phase

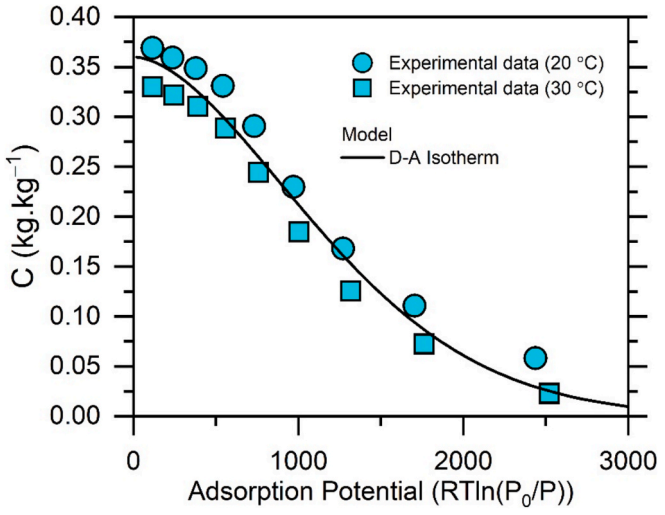

Fig. 4. Characteristic curve of Siogel-water adsorption at 20 °C and 30 °C as a function of adsorption potential. The blue circles and squares represent the experimental adsorption data measured with a vapor sorption analyzer (SPSx-1μ from ProUmid GmbH & Co. KG, Ulm, Germany) at 20 °C and 30 °C, respectively, while the continuous, black line represents the results of the D-A isotherm model fitting. (For interpretation of the references to colour in this figure legend, the reader is referred to the web version of this article.)

Table 4
D-A isotherm regression results for water adsorption on Siogel material.

Parameter	Value	unit
C_0	0.36	kg·kg^{-1}
E	3310	J·mol^{-1}
n	1.74	–

began, feed water came into contact with the adsorbent material, initiating vapor adsorption. This process released the heat of adsorption, which slowed the rate of temperature decrease in the bed until the temperature stabilized at the desired value. Simultaneously, the pressure drop caused by vapor adsorption provided the driving force for more evaporation from the liquid droplets on the bed's side section.

During this phase, the temperature in the feed tank (represented by the continuous green line in Fig. 5a) dropped due to the cooling effect of water evaporation between dimensionless time 0 and approximately 0.25. However, as adsorption progressed and the adsorption material approached saturation, the driving force for adsorption decreased, in turn reducing the evaporation rate. As a result, the feed tank temperature decline slowed. Eventually, the heat transfer from the internal coil in the feed tank (used for temperature control) surpassed the latent heat demand for evaporation, causing the tank temperature to return to its initial setpoint. While the cooling temperature generated (20 °C) in the feed tank as an output of the system would not be suitable for space cooling, it may be utilized for process cooling applications.

At dimensionless time 0.5 (half of the cycle time), a sharp rise in the temperature of bed #1 marked the beginning of the preheating phase. During this phase, the adsorption unit was isolated, and the cooling water in its circuit was replaced with hot water from the heat storage tank. The rapid temperature increase prepared the bed for desorption. Initially, some slight desorption occurred, which increased the bed pressure and counteracted the desorption phenomenon, temporarily limiting the process. The subsequent desorption phase began when the adsorption unit was connected to the distillate tank. High-temperature water in the internal circuit of the bed provided the energy needed for water vapor to desorb from the adsorbent material. The desorbed water vapor was condensed on droplets on the condensing side of the bed and collected in the distillate tank, leading to additional driving force for further water desorption. Mirroring what occurred to the feed tank temperature during adsorption, condensation released heat, causing the distillate tank temperature (dash-dot red line in Fig. 5a) to rise initially. However, as the adsorbent material dried and the driving force for desorption diminished, the desorption rate decreased, resulting in a gradual decline in the distillate tank temperature toward its initial value by the end of the phase.

The temperature evolution of both the feed and distillate tanks followed this cyclic pattern across successive cycles, as shown in Fig. 5a. These temperature changes were synchronized with the cyclic operation of the adsorption beds, ensuring consistent water production throughout the process.

The transient pressures of the adsorption units (beds) shown in Fig. 5b also reflect these cyclic operations. For adsorption unit #1, a sharp drop in pressure was observed at the beginning of the cycle, followed by a stable low-pressure plateau. This behavior is attributed to the

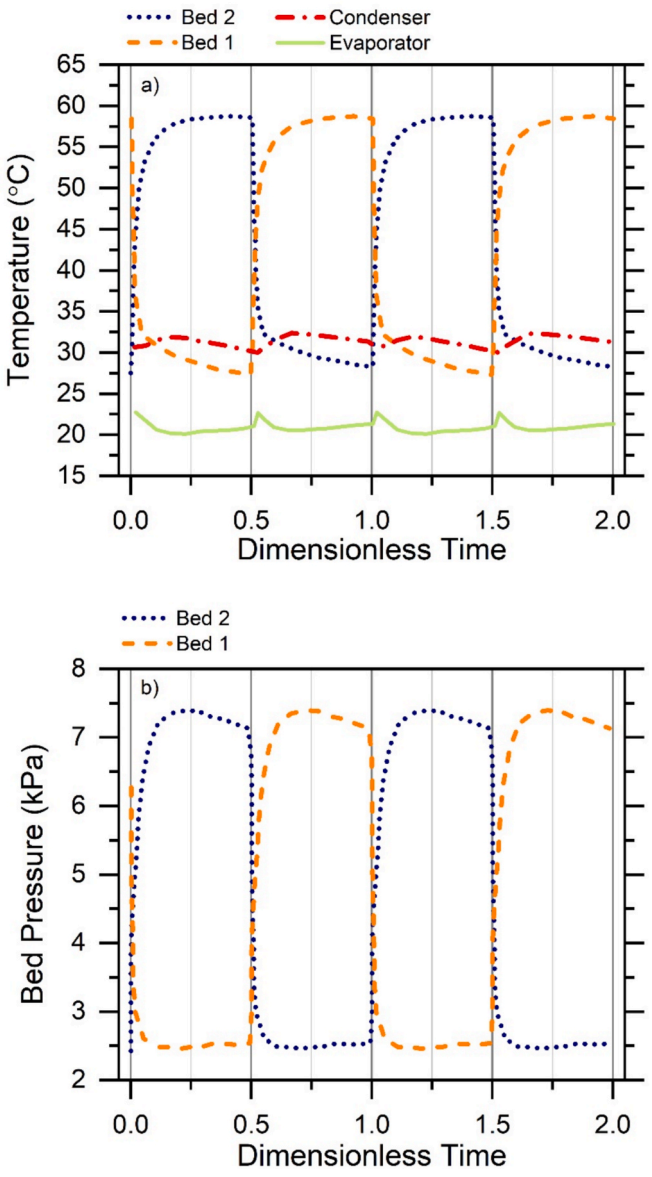

Fig. 5. a) Temperature and b) pressure evolution of the adsorption beds, feed tank (evaporator), and distillate tank (condenser) in two adsorption desalination cycles performed with the hot water temperature set at 60 °C. Note that the x axis displays the dimensionless time, that is, the physical time divided by the total duration of the cycle, the latter equal to 50 min. The plot highlights the trends observed during the various phases of each cycle, regardless of the absolute cycle duration. (T_{amb} = 23 °C).

cooling phase and subsequent adsorption. During the adsorption phase, water vapor was continuously adsorbed by the material, which drove evaporation without causing vapor accumulation in the bed. As a result, the pressure remained nearly constant throughout the adsorption phase until its conclusion. In contrast, the desorption phase exhibited a distinctly different transient pressure. At the start of desorption, there was a rapid pressure increase to a peak value, followed by a gradual decline. Initially, when the adsorbent material contained a large amount of water, the desorption rate exceeded the condensation rate, leading to a buildup of vapor pressure. As the adsorbent material dried, the desorption rate decreased, eventually falling below the condensation rate, resulting in a steady decline in bed pressure. The peak pressure observed in the middle of the desorption phase marks the point where the desorption and condensation rates were nearly equal. This peak is critical for process optimization, as it could be used to maximize water production by adjusting the desorption duration to ending at this point without altering the adsorption phase. Such an optimization might be particularly feasible in systems with more than two adsorption units.

A representative phase diagram of an adsorption desalination cycle is shown in Fig. 6. The diagram consists of the bed temperature and pressure axes, with isosteric lines as the background. The diagonal dotted lines represent the equilibrium water uptake on the adsorbent material, as determined by the Siogel/water adsorption isotherm, ranging from zero to the maximum possible water uptake in fully saturated Siogel. The orange dashed lines, on the other hand, depict the cyclic path of the process under specific conditions: a desorption temperature of 60 °C and a cycle duration of 50 min.

The cyclic progression consists of four distinct phases, beginning with an isosteric path (1) from point A to B. During this phase, the bed temperature and pressure decreased, while the water uptake did not change considerably, which implies a pre-cooling phase in which the bed was isolated and not in contact with the feed water. (2) From point B to C, the system entered the adsorption phase as the feed water droplets run through the evaporation side of the bed. This phase involved crossing the isosteric lines towards saturation, indicating increased water uptake. The phase was almost isobaric consistent with Fig. 5b, due to the dependence of evaporation on adsorption as its driving force, leading to constant pressure. Following the adsorption phase, the system transitioned (3) from point C to D. Here, both bed temperature and pressure increased along an isosteric path, reflecting the preheating phase in the isolated bed. Finally, during the desorption phase (4) from point D to A, the system moved away from the saturation line, crossing the isosteric lines as the adsorbent material became drier. Notably, this phase involved a greater pressure change compared to the adsorption phase, as previously discussed and observed in Fig. 5b.

In addition to representing the bed temperature and pressure, the phase diagram also provides valuable insights into the ideal water production of the cycle. The maximum and minimum water uptake, observable at points B and D respectively, define the net water uptake, or the ideal water production per unit mass of adsorbent. In this case, the value was 0.11 $kg \cdot kg^{-1}$. For a system with 1 ton of adsorbent material operating at the specified cycle duration, the ideal SDWP would be almost 3.17 $m^3 \cdot ton^{-1} \cdot day^{-1}$, which is 27 % higher than the actual SDWP measured based on the collected product water in the distillate tank. The

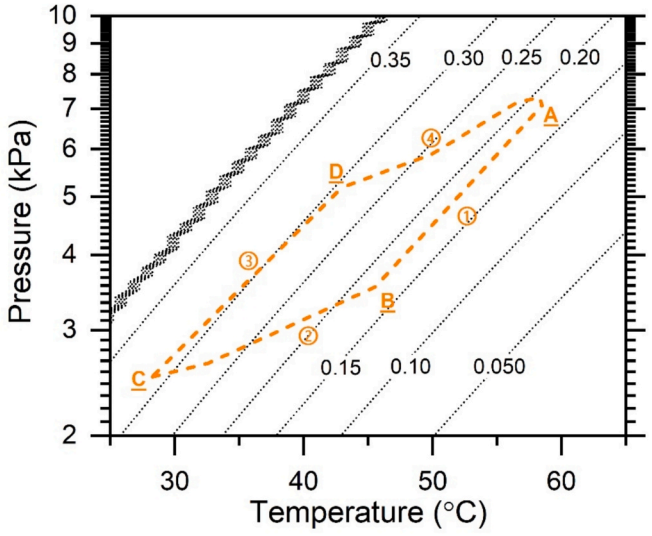

Fig. 6. Phase diagram of one generic adsorption desalination cycle at 60 °C hot water temperature and 50 min cycle duration. The black, diagonal, dotted lines are the isosteric lines calculated from the adsorption isotherm, while the orange, dashed line represents the four phases of the adsorption cycle. ($T_{heat\ source}$ = 62 °C & $T_{heat\ sink}$ = 20 °C). (For interpretation of the references to colour in this figure legend, the reader is referred to the web version of this article.)

discrepancy is mainly due to the fact that the phase diagram accounts only for the equilibrium water uptake determined by the isotherm, neglecting the impact of adsorption kinetics. While the isotherm dictates the maximum potential water uptake, the kinetics determine how quickly these values can be achieved. Therefore, if the cycle duration is sufficiently long to allow equilibrium conditions to be reached, the ideal water production values can be realized. However, longer cycle durations may actually reduce daily water production, as will be discussed below. Overall, the cycle depicted in the phase diagram shown in Fig. 6 is close to the ideal cycle expected from the theoretical adsorption desalination cycle in which the process includes two isosteric and two isobaric steps.

In addition to evaluating the thermodynamic performance and water desalination rate of the adsorption desalination plant, the quality of the product water was also monitored to ensure no or negligible passage of solutes from the feed occurred. In the current configuration, the feed water droplets run continuously through evaporation side of the bed, which is separated by polymeric mesh from both the adsorbent materials and the condensation side. This design necessitated verification that droplets from the feed water did not cross into the distillate side, thus creating a short-circuit. As a primary assessment, two tests were performed in which tap water was used on the feed side. On the distillate side, deionized water was used in the first test as initial (receiving) water solution, while tap water was used in the second. In the first test, the electrical conductivity (EC) of the distillate was expected to remain relatively constant throughout the operation (when water product from the system mixes with distillate water, the EC of the mixture should not change as long as the product water has similar EC of distillate water). In the second test, however, a decrease in EC was anticipated due to dilution of tap water by the less saline product water obtained in the system. Based on the observed change in EC and the obtained volume of product water, the EC of the desalinated water was estimated through mass balance to be approximately 40 μS/cm, which is significantly lower than the feed water EC of 333 μS/cm and corresponds to a product water salinity roughly equal to 20 mg/L, which is well below limits required for drinking water. The conditions and the results of the tests are summarized in the Table S.2 of the SI.

3.3. Sensitivity analyses

The effects of two operating parameters on adsorption desalination performance indicators, namely, SDWP and SCP, were determined experimentally. Firstly, the effect of hot water (desorption) temperature is shown in Fig. 7a. The results imply the strong dependency of the system's performance on the hot water temperature. For example, the SDWP rose to almost 3.8 $m^3 \cdot ton^{-1} \cdot day^{-1}$ by increasing the desorption temperature to 70 °C. This improvement can be attributed to two cumulative effects of higher temperatures. Firstly, as the desorption temperature increases, the equilibrium minimum water uptake is reduced, enabling more water to be desorbed from the adsorbent. Secondly, since adsorption kinetics is a function of temperature, the desorption phase is accelerated. Together, these effects resulted in a more rapid desorption of a larger amount of water from the adsorbent material, in turn translating into increased water production. In addition, a lower equilibrium minimum water uptake leaves the adsorbent drier at the beginning of the subsequent adsorption phase, enhancing its capacity for adsorption. This greater capacity facilitates more effective evaporation from the feedwater, which not only increases water production but also boosts the cooling power of the system, as reflected by higher SCP values. Notably, both SDWP and SCP increased with a sharper slope at higher temperatures, due to the exponential nature of the relation between temperature and water vapor pressure, which is also evident from the adsorption isotherm. All that being said, it is important to note that the energy required for the desorption phase, primarily provided by hot water, constitutes the major energy demand of the system. While solar energy serves as the primary source, minimizing operational costs, any additional energy required during periods without solar power can considerably impact the cost-effectiveness of the system or would require effective energy storage units.

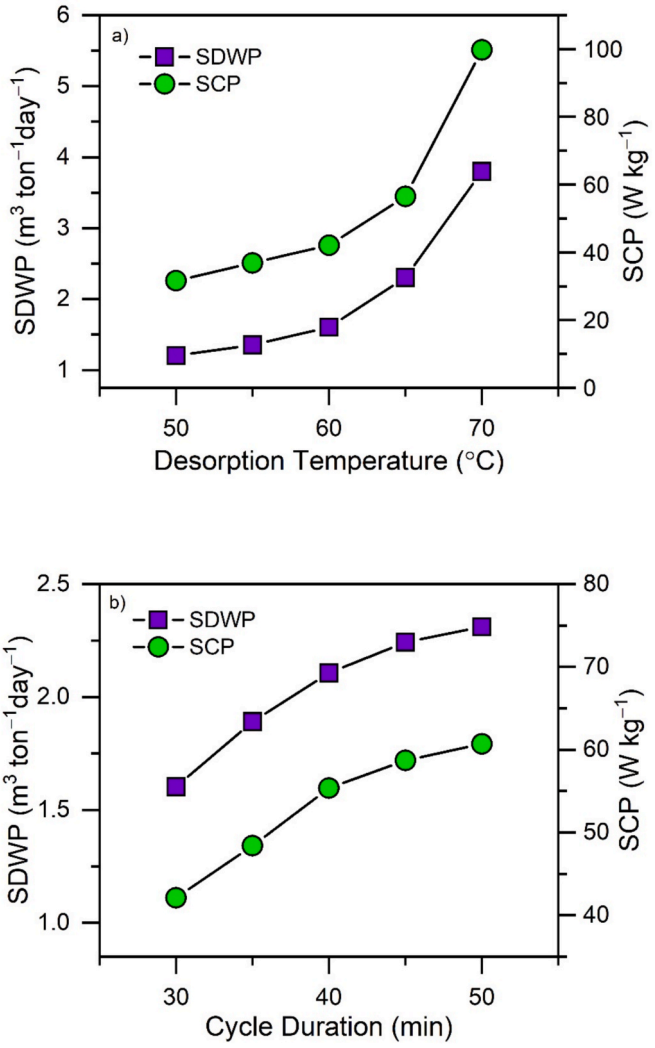

Fig. 7. Effect of a) hot water (desorption) temperature and b) cycle duration on the performance indicators, SDWP and SCP, assessed through desalination experiments. The purple squares represent the value of SDWP and refer to the left-hand axis, while the green circles are SCP values and refer to the right-hand axis. (For interpretation of the references to colour in this figure legend, the reader is referred to the web version of this article.)

The effect of cycle duration on the performance indicators of adsorption desalination, SDWP and SCP, is presented in Fig. 7b. Both indicators increased for longer cycle durations within the range tested in this study. Theoretically, if cycle duration increases even more, an optimal point should be reached when SDWP is maximized (not reached in the current study), beyond which this performance parameter starts to decline for longer cycle duration. Extending the cycle time allowed the system more time to approach the minimum and maximum equilibrium water uptake values, thereby achieving closer-to-ideal water production during each cycle. However, as the adsorbent approaches saturation in the adsorption phase and becomes drier in the desorption phase, the driving force for adsorption and desorption diminishes, resulting in slower rates of water uptake and release. This trade-off is particularly substantial when considering production over time, such as SDWP. Although longer cycle durations improve the amount of water produced per cycle, fewer cycles can be completed in a given time. As a result, the overall production rate initially increases, levels off, and may even

decline if the cycle duration exceeds the optimal point. Moreover, since adsorption transient is influenced by the desorption temperature, the optimal cycle duration for maximizing SDWP depends also on the specific temperature conditions. At each desorption temperature, an optimal balance exists between cycle duration and water production, beyond which performance gains diminish. Ambient conditions also influence this optimal cycle time. For instance, as ambient temperature increases, the desorption temperature achievable via solar panels rises, enabling drier conditions in the adsorbent material and enhancing net water uptake. A higher desorption temperature not only improves adsorption capacity but also accelerates the desorption rate. However, rising ambient temperature may have additional, detrimental effects. As it increases, the dry air cooler may approach its maximum operating capacity, causing the condensation temperature to rise and the condensation rate to decline. This may limit the benefits of elevated desorption temperatures.

Similar to the influence of desorption temperature on SDWP and SCP, Fig. 8a shows that both COP and OCR values increased with higher hot water temperatures. Notably, operating at 70 °C resulted in a COP of 0.56, while the OCR exceeded 1 at temperatures above 68 °C. As previously discussed, increasing the hot water inlet temperature enhances the desorption process, net water uptake, and consequently, the system's desalination and cooling capacities. This leads to higher desorption and evaporation heat powers per cycle, albeit at different rates, resulting in improved COP and OCR values. For OCR values greater than 1, it is essential to clarify that OCR represents the ratio of the combined heat powers of desalination (condenser) and cooling (evaporator) to the desorption heat power supplied. It does not equate to the ratio of total output heat power to total input heat power for the system, as the evaporator's heat power is also an input. Therefore, OCR values exceeding 1 do not violate the first law of thermodynamics but rather indicate a more thermodynamically efficient system. These values signify that, for a given amount of desorption heat supplied, the system achieves greater useful outputs in the form of desalination and cooling. Similarly, Fig. 8b illustrates an increase in both COP and OCR with longer cycle durations. This improvement is attributed to the system approaching adsorption and desorption equilibrium, as defined by the adsorption isotherm. This equilibrium results in higher net water uptake on the adsorbent, leading to greater freshwater production and cooling per cycle. By extending the cycle duration to 50 min, COP nearly reached 0.55, while an OCR of 1.1 was achieved. However, the impact of cycle duration on these indicators beyond the range shown in the graph remains uncertain and requires further investigation.

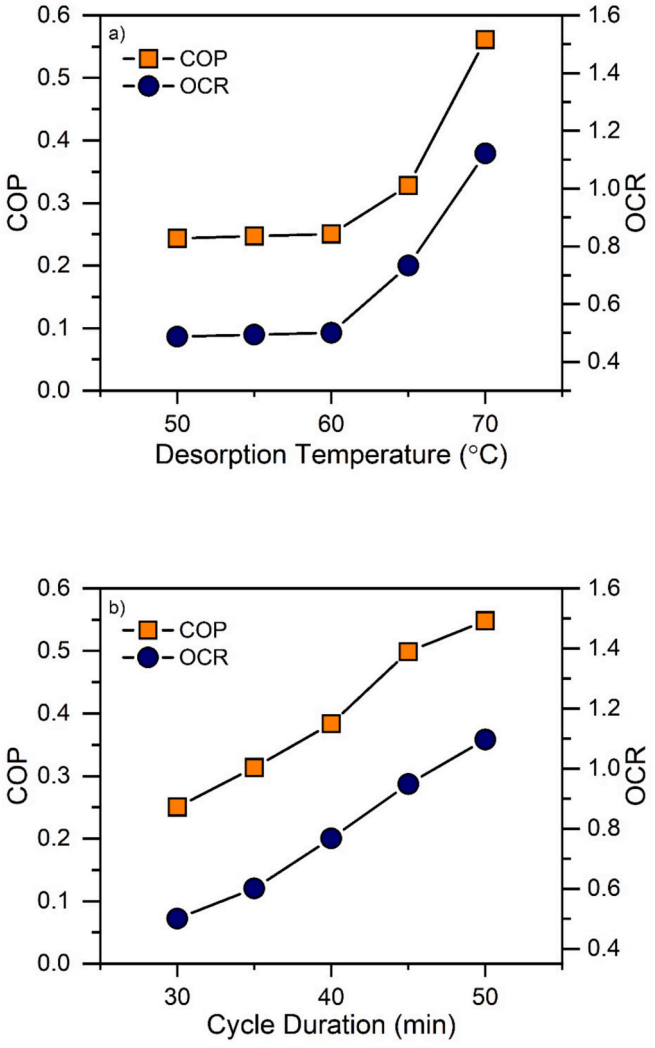

Fig. 8. Effect of a) hot water (desorption) temperature and b) cycle duration on the performance indicators, COP and OCR assessed through desalination experiments. The orange squares represent the value of COP and refer to the left-hand axis, while the blue circles are OCR values and refer to the right-hand axis. (For interpretation of the references to colour in this figure legend, the reader is referred to the web version of this article.)

Moreover, Fig. 9 presents a comparison of the performance of the pilot plant from the current study with other adsorption desalination plants reported in the literature, specifically in terms of specific daily water production (SDWP) relative to plant size (adsorption mass). For this comparison, only experimental results from silica gel-based systems with conventional (non-hybrid and non-advanced configurations, such as heat recovery schemes) designs were included (the data for this comparison taken from the literature with more details is provided in the Table S.3 of the SI as well [10,31,35,36]). These systems were selected based on operating conditions most closely matching those of the current study: bed hot water temperature of 70 °C, bed cold water temperature of 25 °C, and evaporator chilled water temperature of 20 °C. According to the graph, the SDWP of these systems ranges from

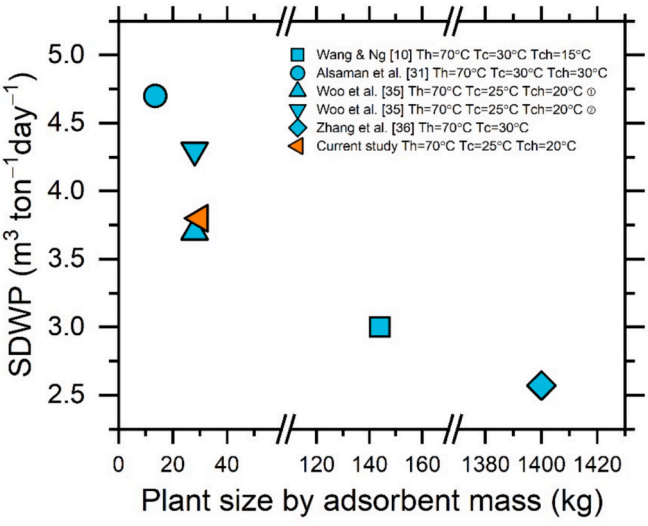

Fig. 9. Performance comparison between the current study and previous works utilizing silica gel-based, conventional, two-bed adsorption desalination systems. The plot shows specific daily water production (SDWP) versus adsorbent mass, used here as a proxy for plant size. Th, Tc, and Tch represent the bed hot water temperature (desorption temperature), bed cold water temperature (adsorption temperature), and evaporator chilled water temperature, respectively. For the production values reported by Woo et al., ① corresponds to the perforated plate feeder system, while ② refers to the spray nozzle feeder evaporator system [10,31,35,36].

2.5 to 4.7 $m^3 \cdot ton^{-1} \cdot day^{-1}$. Notably, the highest SDWP value, reported by Alsaman *et al.* [31] was achieved under higher chilled water temperature in the evaporator (30 °C) compared to other studies, which resulted from higher evaporator and adsorption phase pressure leading to higher net water uptake. Such higher evaporation temperature limits the applicability of cooling production (second output other than desalination) of the system, highlighting a trade-off between desalination and cooling outputs. The performance presented in the current study falls within the higher end of the range, comparable to the results of Woo *et al.* [35] which tested two feeder configurations. To compare the current study and the mentioned study by Woo et al., while both systems worked at the exact same operating conditions, the spray nozzle feeder evaporator configuration showed the highest SDWP. However, it should be noted that the data point from that study was taken at the optimum cycle duration, while the cycle duration for the current study was not optimized and still allow for substantial improvement according to Fig. 8. The graph also highlights a general trend of reduced production capacity as system scale increases, which might be partly due to the increasing water vapor transfer resistance at larger scale. In fact, the larger the system scale, the longer is the path of water vapor molecules from the evaporator to the adsorbents and from the adsorbent to the condenser. A longer path decreases the rate of adsorption and condensation, hence water production. This phenomenon highlights the advantage of the configuration proposed in this work, in which droplet-based water circulation between the tanks and the adsorption beds (feed and product water droplets in the side sections of the beds) reduces the vapor path length, the transfer resistance, and ensures a more consistent production value regardless of the size of the system. Overall, while the scheme in this study reduced vapor transfer resistance and resulted in high SDWP and COP, the production remained within the reported range. This limited improvement may be attributed to heat transfer from the adsorbent section (operating at 50–70 °C) to the product (distillate) water droplets in the distillation side of the bed during desorption (at 25 °C). This unwanted heat transfer could raise the product water temperature, reducing condensation efficiency, net water uptake, and, consequently, SDWP. Further investigations are needed to explore this effect in detail and identify strategies for mitigating it. While a parameter-by-parameter comparison with other systems may not always favor our design, a holistic assessment, including SDWP, COP, and the achieved cooling temperature, indicates its promising potential. Importantly, these results were obtained under non-optimized conditions and at an earlier stage of development relative to other systems. This leaves room for improvement and suggests that, as development progresses, our system may ultimately offer advantages over those previously reported in the literature.

Beyond technical performance, long-term sustainability is a key consideration, especially regarding life-cycle environmental impacts. While a full LCA was beyond this study's scope, relevant insights can be drawn from related sorption systems. Thu et al. [37] estimated that adsorption desalination at a 1000 $m^3 \cdot day^{-1}$ scale could reduce CO_2 emissions by ~3 $kg \cdot m^{-3}$ versus reverse osmosis, though upstream and infrastructure impacts were not considered. Broader LCAs of sorption-based thermal energy storage (Horn et al. [38]; Niemborg et al. [39]) highlight high embodied energy and global warming potential from adsorbent production—offset only through long service lifetimes and frequent cycling. Similarly, Hayatina et al. [40] found that thermochemical storage materials often carry large production footprints, requiring extended operation to achieve net benefits. These findings suggest that sorption desalination may face similar trade-offs. Still, compared to energy- or component-intensive methods like RO and MSF, sorption systems can offer lower life-cycle impacts by leveraging solar or waste heat and durable, regenerable adsorbents. A full system-level LCA remains essential to assess these benefits under real-world conditions.

When considering system scale-up, several challenges must still be addressed, including the trade-off between hydraulic complexity and modularity, increased pressure drops and mass transfer limitations in larger beds, long-term vacuum maintenance, and the need for durable materials, such as stainless steel, to prevent degradation and ensure operational reliability. A key concern is the structural resilience of mesh-packed beds, which may face issues such as deformation, packing instability, and reduced heat transfer as system size increases. While such problems were not observed at pilot scale, future designs could mitigate them by adopting more robust support configurations—such as metallic heat exchangers with coated adsorbents or perforated plates [41]—already common in commercial adsorption chillers. Additionally, advanced packing geometries like 3D-printed TPMS lattices [42] can improve mechanical integrity and surface area retention. Combined with stronger vacuum systems and precise cycle control [43], these strategies can support scale-up without sacrificing performance.

Finally, to assess the system's energy consumption and losses, a representative case was analyzed using a desorption temperature of 70 °C and an adsorption cycle duration of 30 min. The analysis showed that each cycle consumed approximately 3.65 kWh of energy, while 3.38 kWh was released as adsorption or condensation heat. This corresponds to an energy loss of about 0.27 kWh per cycle, representing roughly 7 % of the total energy input. When powered by the solar system, the required input energy drops to approximately 0.65 kWh per cycle. Detailed assumptions, calculations, and results are provided in Tables S4 and S5 and Fig. S3 of the SI.

4. Conclusions

The performance of a solar-driven pilot-scale adsorption desalination plant utilizing Siogel adsorbent material and employing a new droplet-based mechanism of feed and distillate water circulation between both tanks and the adsorption beds was investigated. The Siogel material was characterized, and its adsorption isotherm model was determined. The system's conventional cycles were tested, with results presented and analyzed in terms of transient temperatures and pressures, as well as the cycle phase diagram. Key performance indicators, including specific daily water production (SDWP), specific cooling production (SCP), coefficient of performance (COP), and overall conversion ratio (OCR), were evaluated. Additionally, the effects of desorption temperature and cycle duration on system performance were experimentally assessed.

The Siogel adsorbent demonstrated comparable performance to other silica gel variants reported in the literature. The system achieved a water production capacity of approximately 3.8 $m^3 \cdot ton^{-1} \cdot day^{-1}$ and a cooling capacity of 100 $W \cdot kg^{-1}$ at a desorption temperature of 70 °C supplied by a solar water heating system, with a cycle duration of 30 min. The study revealed that optimizing cycle duration could further enhance SDWP. Higher desorption temperatures, facilitated by the solar heating system, improved both water and cooling production. Although performance metrics improved with increasing cycle duration, the improvement showed diminishing returns. The findings suggest that the droplet-based circulation scheme facilitated water vapor transfer from the feed water to the adsorbent and from the adsorbent to the distillate water flow, allowing a consistent performance regardless of system size. However, this positive effect may have been partially offset by heat transfer from the adsorption bed during the desorption phase to the circulating distillate water, which slightly increased its temperature and potentially reduced water vapor condensation efficiency.

Overall, when considering together SDWP, COP, and the achieved cooling temperature in relation to the system's current operating conditions and stage of development, the design presented in this work demonstrates promising potential compared to earlier approaches. The results uphold the feasibility of scalable solar-driven adsorption desalination systems and highlight the considerable impact of operating parameters observed in bench-scale studies, also on the performance of pilot-scale plants. The system's flexibility suggests substantial potential for optimization, underscoring the importance of continued experimentation and advanced modeling efforts by the research community.

CRediT authorship contribution statement

Ali Naeimi Tabasian: Writing – original draft, Visualization, Validation, Investigation, Formal analysis. **Alberto Saija:** Writing – review & editing, Investigation. **Matteo Morciano:** Writing – review & editing, Validation, Supervision, Formal analysis, Conceptualization. **Matteo Fasano:** Writing – review & editing, Supervision, Project administration, Funding acquisition, Formal analysis, Conceptualization. **Alberto Tiraferri:** Writing – review & editing, Supervision, Resources, Funding acquisition. **Eliodoro Chiavazzo:** Writing – review & editing, Supervision, Project administration, Methodology, Data curation, Conceptualization.

Declaration of competing interest

The authors declare the following financial interests/personal relationships which may be considered as potential competing interests: Matteo Fasano reports financial support was provided by Ministry of Education and Merit. If there are other authors, they declare that they have no known competing financial interests or personal relationships that could have appeared to influence the work reported in this paper.

Acknowledgments

The authors would like to thank Walter Mittelbach, Gabriele Penello, and Matteo Calò from Sorption Technologies GmbH for useful discussions. We also thank Alessio Mondello for supporting the DVS analyses and Giovanni Luchesi for helping with water quality tests. This study was carried out within the WADERE project – funded by the Ministero dell'Università e della Ricerca – within the PRIN 2022 program (D. D.104 – 02/02/2022). This manuscript reflects only the authors' views and opinions and the Ministry cannot be considered responsible for them. Authors are grateful to Clean Water Center@Polito for funding.

Appendix A. Supplementary data

Supplementary data to this article can be found online at https://doi.org/10.1016/j.enconman.2025.120190.

Data availability

Data will be made available on request.

References

[1] Bigas H. Water security and the global water agenda: a UN-water analytical brief. United Nations University-Institute for Water, Environment and Health; 2013.
[2] Ng KC, Thu K, Kim Y, Chakraborty A, Amy G. Adsorption desalination: an emerging low-cost thermal desalination method. Desalination 2013;308:161–79. https://doi.org/10.1016/j.desal.2012.07.030.
[3] Alsaman AS, Askalany AA, Harby K, Ahmed MS. A state of the art of hybrid adsorption desalination–cooling systems. Renew Sustain Energy Rev 2016;58:692–703. https://doi.org/10.1016/j.rser.2015.12.266.
[4] Warsinger DM, Mistry KH, Nayar KG, Chung HW, Lienhard JH. Entropy generation of desalination powered by variable temperature waste heat. Entropy 2015;17:7530–66.
[5] Ehrenman G. From sea to sink. Mech Eng 2004;126:38–43. https://doi.org/10.1115/1.2004-OCT-3.
[6] Sanap DB, Kadam KD, Narayan M, Kasthurirangan S, Nemade PR, Dalvi VH. Analysis of saline water desalination by directed solvent extraction using octanoic acid. Desalination 2015;357:150–62. https://doi.org/10.1016/j.desal.2014.11.020.
[7] Janajreh I, Zhang H, El Kadi K, Ghaffour N. Freeze desalination: current research development and future prospects. Water Res 2023;229:119389. https://doi.org/10.1016/j.watres.2022.119389.
[8] Giagnorio M, Morciano M, Zhang W, Hélix-Nielsen C, Fasano M, Tiraferri A. Coupling of forward osmosis with desalination technologies: System-scale analysis at the water-energy nexus. Desalination 2022;543:116083. https://doi.org/10.1016/j.desal.2022.116083.
[9] Morciano M, Malaguti M, Ricceri F, Tiraferri A, Fasano M. Process optimization of osmotic membrane distillation for the extraction of valuable resources from water streams. NPJ Clean Water 2024;7:1. https://doi.org/10.1038/s41545-023-00294-2.
[10] Wang X, Ng KC. Experimental investigation of an adsorption desalination plant using low-temperature waste heat. Appl Therm Eng 2005;25:2780–9. https://doi.org/10.1016/j.applthermaleng.2005.02.011.
[11] Wu JW, Biggs MJ, Pendleton P, Badalyan A, Hu EJ. Experimental implementation and validation of thermodynamic cycles of adsorption-based desalination. Appl Energy 2012;98:190–7. https://doi.org/10.1016/j.apenergy.2012.03.022.
[12] Hua WS, Xu HJ, Xie WH. Review on adsorption materials and system configurations of the adsorption desalination applications. Appl Therm Eng 2022;204:117958. https://doi.org/10.1016/j.applthermaleng.2021.117958.
[13] Morciano M, Fasano M, Bergamasco L, Albiero A, Lo Curzio M, Asinari P, et al. Sustainable freshwater production using passive membrane distillation and waste heat recovery from portable generator sets. Appl Energy 2020;258:114086. https://doi.org/10.1016/j.apenergy.2019.114086.
[14] De Angelis P, Tuninetti M, Bergamasco L, Calianno L, Asinari P, Laio F, et al. Data-driven appraisal of renewable energy potentials for sustainable freshwater production in Africa. Renew Sustain Energy Rev 2021;149:111414. https://doi.org/10.1016/j.rser.2021.111414.
[15] Moneer AA, Elewa MM. The innovative technologies for desalination and their cost benefits. Egypt J Aquat Res 2024.
[16] Thu K, Saha BB, Chakraborty A, Chun WG, Ng KC. Study on an advanced adsorption desalination cycle with evaporator–condenser heat recovery circuit. Int J Heat Mass Transf 2011;54:43–51. https://doi.org/10.1016/j.ijheatmasstransfer.2010.09.065.
[17] Ng KC, Thu K, Saha BB, Chakraborty A. Study on a waste heat-driven adsorption cooling cum desalination cycle. Int J Refrig 2012;35:685–93. https://doi.org/10.1016/j.ijrefrig.2011.01.008.
[18] Youssef PG, Mahmoud SM, Al-Dadah RK. Effect of evaporator temperature on the performance of water desalination/refrigeration adsorption system using AQSOA-ZO2. Int J Environ Chem Ecol Geol Eng 2015;9:679–83.
[19] Wu JW, Hu EJ, Biggs MJ. Thermodynamic analysis of an adsorption-based desalination cycle (part II): effect of evaporator temperature on performance. Chem Eng Res Des 2011;89:2168–75. https://doi.org/10.1016/j.cherd.2010.12.012.
[20] Mitra S, Srinivasan K, Kumar P, Murthy SS, Dutta P. Solar driven adsorption desalination system. Energy Proc 2014;49:2261–9. https://doi.org/10.1016/j.egypro.2014.03.239.
[21] Thu K, Chakraborty A, Kim Y-D, Myat A, Saha BB, Ng KC. Numerical simulation and performance investigation of an advanced adsorption desalination cycle. Desalination 2013;308:209–18. https://doi.org/10.1016/j.desal.2012.04.021.
[22] Thu K, Saha BB, Chua KJ, Ng KC. Performance investigation of a waste heat-driven 3-bed 2-evaporator adsorption cycle for cooling and desalination. Int J Heat Mass Transf 2016;101:1111–22. https://doi.org/10.1016/j.ijheatmasstransfer.2016.05.127.
[23] Youssef PG, Mahmoud SM, Al-Dadah RK. Numerical simulation of combined adsorption desalination and cooling cycles with integrated evaporator/condenser. Desalination 2016;392:14–24. https://doi.org/10.1016/j.desal.2016.04.011.
[24] Ali SM, Haider P, Sidhu DS, Chakraborty A. Thermally driven adsorption cooling and desalination employing multi-bed dual-evaporator system. Appl Therm Eng 2016;106:1136–47. https://doi.org/10.1016/j.applthermaleng.2016.06.045.
[25] Naeimi A, Nowee SM, Akhlaghi Amiri HA. Numerical simulation and theoretical investigation of a multi-cycle dual-evaporator adsorption desalination and cooling system. Chem Eng Res Des 2020;156:402–13. https://doi.org/10.1016/j.cherd.2020.02.016.
[26] Amirfakhraei A, Zarei T, Khorshidi J. Performance improvement of adsorption desalination system by applying mass and heat recovery processes. Therm Sci Eng Prog 2020;18:100516. https://doi.org/10.1016/j.tsep.2020.100516.
[27] Ma H, Zhang J, Liu C, Lin X, Sun Y. Experimental investigation on an adsorption desalination system with heat and mass recovery between adsorber and desorber beds. Desalination 2018;446:42–50. https://doi.org/10.1016/j.desal.2018.08.022.
[28] Bai S, Ho TC, Ha J, An AK, Tso CY. Study of the salinity effects on the cooling and desalination performance of an adsorption cooling cum desalination system with a novel composite adsorbent. Appl Therm Eng 2020;181:115879. https://doi.org/10.1016/j.applthermaleng.2020.115879.
[29] Du B, Gao J, Zeng L, Su X, Zhang X, Yu S, et al. Area optimization of solar collectors for adsorption desalination. Sol Energy 2017;157:298–308. https://doi.org/10.1016/j.solener.2017.08.032.
[30] Ali ES, Harby K, Askalany AA, Diab MR, Alsaman AS. Weather effect on a solar powered hybrid adsorption desalination-cooling system: a case study of Egypt's climate. Appl Therm Eng 2017;124:663–72. https://doi.org/10.1016/j.applthermaleng.2017.06.048.
[31] Alsaman AS, Askalany AA, Harby K, Ahmed MS. Performance evaluation of a solar-driven adsorption desalination-cooling system. Energy 2017;128:196–207. https://doi.org/10.1016/j.energy.2017.04.010.
[32] Kyaw THU. Adsorption desalination: theory & experiments; 2010.
[33] Dubinin MM. The potential theory of adsorption of gases and vapors for adsorbents with energetically nonuniform surfaces. Chem Rev 1960;60:235–41. https://doi.org/10.1021/cr60204a006.
[34] Stoeckli F. Recent developments in Dubinin's theory. Carbon 1998;36:363–8. https://doi.org/10.1016/S0008-6223(97)00194-2.
[35] Woo S-Y, Lee H-S, Ji H, Moon D-S, Kim Y-D. Silica gel-based adsorption cooling cum desalination system: focus on brine salinity, operating pressure, and its effect on performance. Desalination 2019;467:136–46. https://doi.org/10.1016/j.desal.2019.06.016.

[36] Zhang H, Ma H, Liu S, Wang H, Sun Y, Qi D. Investigation on the operating characteristics of a pilot-scale adsorption desalination system. Desalination 2020; 473:114196. https://doi.org/10.1016/j.desal.2019.114196.
[37] Thu K, Chakraborty A, Saha BB, Chun WG, Ng KC. Life-cycle cost analysis of adsorption cycles for desalination. Desalin Water Treat 2010;20:1–10. https://doi.org/10.5004/dwt.2010.1187.
[38] Horn R, Burr M, Fröhlich D, Gschwander S, Held M, Lindner J, et al. Life cycle assessment of innovative materials for thermal energy storage in buildings. Proc CIRP 2018;69:206–11. https://doi.org/10.1016/j.procir.2017.11.095.
[39] Nienborg B, Helling T, Fröhlich D, Horn R, Munz G, Schossig P. Closed adsorption heat storage—a life cycle assessment on material and component levels. Energies 2018;11:3421.
[40] Hayatina I, Auckaili A, Farid M. Review on the life cycle assessment of thermal energy storage used in building applications. Energies 2023;16:1170.
[41] Freni A, Calabrese L, Malara A, Frontera P, Bonaccorsi L. Silica gel microfibres by electrospinning for adsorption chillers. Energy 2019;187:115971. https://doi.org/10.1016/j.energy.2019.115971.
[42] Gado MG, Al-Ketan O, Aziz M, Al-Rub RA, Ookawara S. Triply periodic minimal surface structures: design, fabrication, 3D printing techniques, state-of-the-art studies, and prospective thermal applications for efficient energy utilization. Energ Technol 2024;12:2301287.
[43] Wang DC, Xia ZZ, Wu JY, Wang RZ, Zhai H, Dou WD. Study of a novel silica gel–water adsorption chiller. Part I. Design and performance prediction. Int J Refrig 2005;28:1073–83. https://doi.org/10.1016/j.ijrefrig.2005.03.001.